Artificial Photosynthesis: Fundamentals, Challenges, and Strategies

Davin Philo, Hamza El-Hosainy, Shunqin Luo, Hao Huang, Fumihiko Ichihara, and Jinhua Ye

1 Introduction

Natural photosynthesis (NPS) is a chemical process conducted by green plants, photosynthetic bacteria, and all other photosynthetic organisms, where CO_2 and water are transformed into carbohydrates and molecular oxygen, respectively [1, 2]. This process can be considered as the most efficient and effective method of converting light energy into chemical energy. Over billions of years, NPS has provided an overwhelming amount of energy stock, mostly in the form of fossil fuels, for the world [3]. However, as is widely known, the rate of depletion of this energy stock is much higher than the rate at which nature can replenish it [2, 4]. Consequently, it is only a matter of time before fossil fuels finally run out. With this looming energy crisis, many approaches have been made to imitate NPS by artificially utilizing light energy to drive the thermodynamically uphill reactions of abundant substances to produce energy-containing chemicals, such as hydrogen, hydrocarbons, and ammonia [1, 3]. At present, this method is known as artificial photosynthesis (APS) or the so-called photocatalytic process [5].

As is widely known, the green chlorophyll pigment plays a major role in the NPS reaction. Generally, light energy or photons are absorbed by chlorophyll and used to remove electrons from water molecules to produce oxygen gas as follows:

$$2H_2O \xrightarrow{light} O_2 + 4H^+ + 4e^-. \quad (1)$$

This oxidation reaction occurs in the reaction center of photosystem II. Afterwards, the freed hydrogen and electrons are transferred to photosystem I and trigger the reduction of carbon dioxide (CO_2) to produce sugar ($C_6H_{12}O_6$) through the Calvin

D. Philo · H. El-Hosainy · S. Luo · H. Huang · F. Ichihara · J. Ye (✉)
International Center for Materials Nanoarchitectonics (WPI-MANA), National Institute for Materials Science (NIMS), 1-1 Namiki, Tsukuba 305-0044, Ibaraki, Japan
e-mail: Jinhua.YE@nims.go.jp

Y. Wakayama and K. Ariga (eds.), *System-Materials Nanoarchitectonics*,
NIMS Monographs, https://doi.org/10.1007/978-4-431-56912-1_14

cycle:

$$CO_2 + 4H^+ + 4e^- \xrightarrow{light} \frac{1}{6}C_6H_{12}O_6 + H_2O. \tag{2}$$

The overall reaction of NPS is written as

$$CO_2 + H_2O \xrightarrow{light} \frac{1}{6}C_6H_{12}O_6 + O_2. \tag{3}$$

Meanwhile, in APS, a material called a photocatalyst (mostly a semiconductor) is usually employed to harvest light energy [5]. Similar to NPS, this photon energy is used by the photocatalyst to generate charge carriers or excitons, i.e., electrons (e^-) and holes (h^+). In detail, upon light illumination, e^- is excited from the valence band (VB) to the conduction band (CB) of the photocatalyst, leaving behind the h^+ in the valence band region [6]. These charge carriers are transferred separately to different reaction centers, where they trigger some endothermic redox reactions; electrons drive the reduction reaction while holes drive the oxidation reaction as follows:

$$A + e^- \xrightarrow{light} A^-, \tag{4}$$

$$D + h^+ \xrightarrow{light} D^+. \tag{5}$$

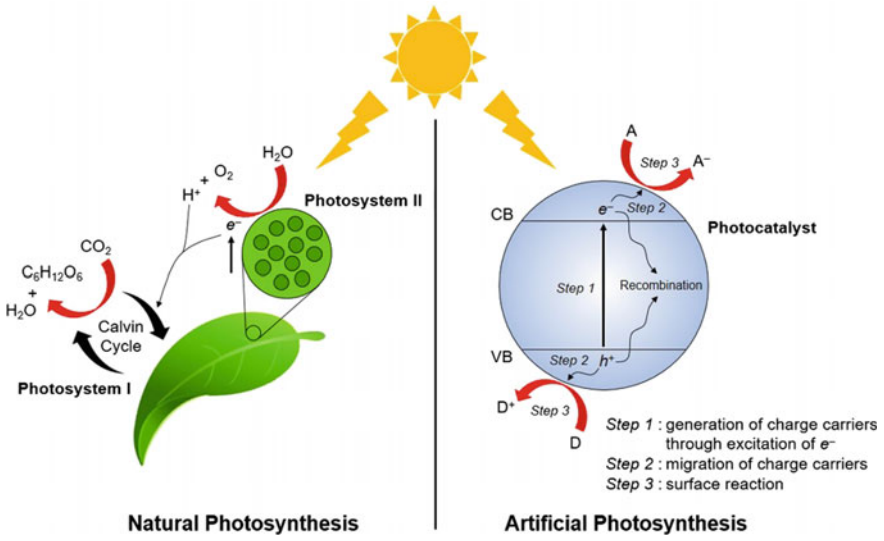

Fig. 1 Comparison between natural and artificial photosynthesis

A and D represent an electron acceptor and electron donor, respectively. Figure 1 illustrates a comparison between NPS and APS.

In the past few decades, many studies have been carried out to obtain a full understanding of the reaction mechanisms, kinetics, substances involved, and other important properties of NPS [5]. Even though we do not yet have sufficient understanding to further proceed to the industrial stage, much progress has been made toward applying the key features of NPS to APS [7]. To date, there are three very well known APS reactions that have attracted considerable attention from scientists and researchers worldwide, i.e., water (H_2O) splitting, carbon dioxide (CO_2) reduction, and nitrogen (N_2) fixation; water, CO_2, and N_2 are very suitable raw materials for APS applications because they are abundant and easily obtained from the natural environment. In this chapter, we provide a summary of the principles, requirements, and latest developments of APS-based reactions.

Before proceeding with the above-mentioned discussion, it is necessary to define a general term that is often used to evaluate photocatalytic efficiency for any APS reaction, i.e., apparent quantum yield (AQY). The concept of AQY has been widely used to make valid comparisons between different experimental and illumination conditions [6]. AQY is evaluated for a certain photon wavelength (monochromatic) and calculated as

$$\mathrm{AQY} = \mathrm{nr}/\mathrm{I}, \tag{6}$$

where n, r, and I represent the number of e^- involved in the photocatalytic reaction, the corresponding production rate, and the rate of incident photons, respectively. Typically, the wavelength-dependent AQY follows the optical absorbance pattern of the semiconductor, which decreases as the irradiation wavelength approaches the absorption edge because of the lower absorption coefficients and larger migration distances for photogenerated carriers [6].

2 Requirements for Artificial Photosynthesis

Since the purpose of APS is to drive some thermodynamically uphill reactions, there are some principal conditions that must be fulfilled so that the reaction may occur effectively and efficiently. These requirements apply to all APS reactions, and therefore, it is important to identify them as the very first stepping stones toward designing any photocatalytic system.

2.1 Thermodynamic Boundaries and Photon Absorption

To successfully perform any redox reaction, one needs to pay careful attention to the thermodynamic constraints of the reaction. In this case, we mostly use the term reduction potential to quantify the thermodynamic state of a certain reaction. The reduction potential or electrode potential is usually defined as a value for measuring the tendency of some substances to receive electrons, and thus be reduced. It is measured as the energy level, with volt (V) as the unit, with respect to a certain standard potential, such as the standard hydrogen electrode (SHE).[1] The higher (more negative) the value of this potential, the greater the likelihood of the species acquiring electrons and being reduced. In contrast, the lower (more positive) this value, the greater the tendency for the backward reaction (oxidation) of the species to occur. For a redox photon-induced reaction to occur, the CB energy level of the photocatalyst must be higher than the potential of the reduction reaction, while the VB must be located at a more positive potential than the oxidation reaction. Since different reactions require different thermodynamic boundaries, some photocatalysts will be suitable for a certain reaction but might not be suitable for other reactions. However, it is also possible to shift the position of the energy band by introducing some impurities, known as dopants, to meet different thermodynamic requirements [8]. More details of the thermodynamic constraints of each APS reaction and the corresponding implications will be presented in later sections.

Furthermore, since the ultimate aim of APS is to utilize the energy emitted by the sun, we also need to consider the characteristics of sunlight itself. The sun emits a spectrum of electromagnetic waves with a relatively broad wavelength, which comprises 3–5% UV (<400 nm), 42–43% visible light (400–700 nm), and 52–55% infrared (>700 nm) [9]. Thus, the utilization of visible light, near infrared (NIR), and infrared is essential to achieving substantial solar energy conversion, although this is more challenging. We often use the term band gap (E_g) to evaluate the light-harvesting ability of a semiconductor photocatalytic material. In the electronic structure of solid materials, including semiconductors, the band gap is usually defined as the energy difference between the top of the valence band (valence band maximum, VBM) and the bottom of the conduction band (conduction band minimum, CBM). The value of E_g is usually obtained by applying the Kubelka–Munk transformation and can be used to determine the maximum wavelength of light (λ_{max}) that the photocatalyst can absorb using the following equation:

$$\lambda_{\max} = hc/E_g, \tag{7}$$

where h is Planck's constant (6.626×10^{-34} m^2 kg/s) and c is the speed of light (3×10^8 m/s). Generally, a photocatalyst can absorb light with a higher energy than its band gap, or in other words, a wavelength less than the value of λ_{max} calculated as

[1] In SHE, the standard electrode potential (E°) of H^+/H_2 is assumed to be 0, where the pressure of hydrogen gas is 1 bar and the activity of H^+ in the solution is equal to 1 (in short, pH 0).

Table 1 List of popular and potential semiconductors that have been applied in APS

Semiconductor	Band gap (eV)	Photocatalytic applications
TiO_2	3.2	Water splitting [12–15], CO_2 reduction [16–18], N_2 fixation [19–21]
$SrTiO_3$	3.2	Water splitting [22–24], CO_2 reduction [25], N_2 fixation [26, 27]
ZnO	3.4	Water splitting [28, 29], CO_2 reduction [30, 31]
$BiVO_4$	2.4	Water splitting[a] [32, 33], CO_2 reduction [34]
WO_3	2.8	Water splitting[a] [32, 35], CO_2 reduction [36, 37]
GaN	3.5	Water splitting [28, 38], CO_2 reduction [39]
GaP	2.2	Water splitting[b] [40, 41], CO_2 reduction [42, 43]
TaON	2.5	Water splitting [44, 45]
Cu_2O	2.0–2.2	Water splitting [46, 47]
CdS	2.4	Water splitting[c] [48–50], CO_2 reduction [51, 52], N_2 fixation [53, 54]
ZnS	3.7	Water splitting[c] [55, 56], CO_2 reduction [57–59]
CoO	2.6	Water splitting [60, 61]
g-C_3N_4	2.7	Water splitting [62–65], CO_2 reduction [66–68], N_2 fixation [69]
Black Phosphorus	0.45–0.76	Water splitting[b] [70]
BiOCl	3.3	N_2 fixation [71, 72]
BiOBr	2.8–2.9	N_2 fixation [73, 74]

[a]only for water oxidation (O_2 production); [b]only for water reduction (H_2 production); [c]mostly for H_2 production owing to the instability of the material

above. Hence, to enable the absorption of a larger proportion of the solar spectrum, a semiconductor with a smaller band gap is preferred. Table 1 shows a list of some semiconductors that have been applied in APS and their corresponding band gaps.

Given that some semiconductors have relatively large band gaps, some approaches to band-gap narrowing have involved inserting some dopant(s) into the molecular arrangement of a semiconductor, thus modifying its electronic structure. The basic concept of this method is to introduce a new energy level below or above the constituent orbital state [10], so that it may change the position of the CBM or VBM, which is also beneficial for meeting different thermodynamic requirements of different reactions as mentioned earlier [8]. For example, one can shift the VBM level of some oxide materials (usually consisting of the O_{2p} state) upwards by adding nitrogen as a dopant, thus introducing the new N_{2p} state, which lies above the O_{2p} state, and generating a higher VBM position [11]. On the other hand, this doping method also has the drawback that the doping sites can act as recombination centers for charge carriers [11]. Therefore, in the design of photocatalytic materials, one must strive to achieve a balance between the modulation of light absorption and the recombination probability [10].

2.2 Charge Carrier Dynamics in Light-Harvesting Material

Following the generation of charge carriers due to photon absorption, the electron–hole pairs need to be separated immediately and transported into different zones; otherwise, they will recombine with each other within the photocatalyst [75, 76]. This electron–hole recombination usually results in a significant loss of energy, thus limiting the quantum efficiency of the photocatalytic system [5]. Consequently, the migration step, which is strongly correlated with the charge carrier dynamics, plays an essential role in an effective photocatalytic system. There are two parameters that are usually used to characterize the charge carrier dynamics of a semiconductor: carrier lifetime and diffusion length [76]. The carrier lifetime can be described as the average time taken for the charge carriers to recombine, whereas the diffusion length is defined as the distance that the carriers can travel before they recombine. From these definitions, it can be easily understood that the higher their values, the higher the probability that the charge carriers reach the surface of the photocatalyst and subsequently participate in the surface reactions. Hence, extensive effort has been made to improve these values, i.e., (1) controlling the shape, structure, and size of the photocatalysts to reduce the distance that the charge carriers must travel before reaching the surface of the photocatalyst; (2) formation of a homojunction and heterojunction to promote the spatial separation of electrons and holes; (3) utilization of a sacrificial agent as a scavenger of particular charge carriers, thus increasing the proportion of oppositely charged carriers in the photocatalyst; and (4) introduction of a cocatalyst on the surface of a photocatalyst that can provide charge accumulation centers and also accelerate interfacial reaction kinetics [5, 75, 77].

2.3 Existence of Reactive Sites

Last but not least, a photocatalyst material should have active catalytic sites on its surface for the APS reaction to occur. However, most photocatalyst surfaces are not typically designed to catalyze redox reactions [76]. To address this problem, a cocatalyst that can provide reactive sites for a certain APS reaction is frequently loaded and dispersed on the surface of the photocatalyst [78]. For this purpose, cocatalyst components are often adapted from the components of electrocatalysts applied for the same reactions [10]. In other cases, some surface defects are introduced on the surface of the photocatalyst, which can unexpectedly provide reactive sites for APS reactions, especially CO_2 reduction [59, 79, 80] and N_2 fixation reactions [69, 71, 73].

To establish effective surface reactions, the reactive sites must be designed according to the Sabatier principle,[2] which states that the catalytic surface must have a trade-off between being reactive and not being poisoned by the reaction intermediates [81]. Hence, the interactions between the sites and the substances (either

[2] This is often associated with the activity volcano plots used to evaluate the adsorption–desorption property of any metal (since most of the active sites for the APS reaction are metal atoms) [78].

the reactant or the product) should be modest: neither too weak so that the sites can adequately bind the reactant and the surface reaction (through the electron transfer process) may take place, nor too strong so that the product can easily desorb from the catalytic surface [82–84]. Secondly, if a cocatalyst is employed, it should form a good coordination with the semiconductor to ensure smooth charge migration into and from the reactive sites [10, 50]. This is because, for any catalytic reaction, a sustained charge carrier supply is the key to a continuous and effective surface reaction [85]. Accordingly, a suitable loading method and a precursor of the cocatalyst are crucial. Finally, increasing the number of reactive sites by either altering the morphology of the material to a low-dimensional structure [48, 86, 87], exposing more active edges of the cocatalyst [88, 89], or reducing the size of the cocatalyst into clusters [90–92] or single atoms [64, 93–95] is also an effective way of enhancing the photocatalytic activity.

Recently, an advanced strategy to satisfy such requirements has been demonstrated by downsizing transition-metal-based cocatalysts to the molecular scale, thus maximizing the catalytic activity [50]. By anchoring well-dispersed single-site Co/Ni species on a sulfide semiconductor, excellent photocatalytic H_2 production was achieved, with AQY as high as 56.2 and 67.5% at 420 nm for Co and Ni species, respectively. These outcomes indicate the importance of the good dispersion of cocatalyst species as well as good coordination between the cocatalyst and the semiconductor, which will result in the full utilization of reactive sites, efficient charge transfer, and favorable kinetics for better catalytic performance [50].

3 Water Splitting

Following the pioneering work of photo-electrochemical water splitting by Fujishima and Honda in the early 1970s [12], much effort has been made toward developing an effective and efficient water-splitting photocatalytic system. Water splitting itself is an uphill redox reaction with an increase in Gibbs free energy (ΔG°) of about 237.13 kJ/mol [78], which can be written as

$$2H_2O \xrightarrow{light} 2H_2 + O_2 \tag{8}$$

The water splitting reaction can be divided into two half reactions, i.e., a hydrogen evolution reaction (HER) and an oxygen evolution reaction (OER):

$$2H^+ + 2e^- \rightarrow H_2, \tag{9}$$

$$2H_2O + 4h^+ \rightarrow O_2 + 4H^+. \tag{10}$$

As already explained for the thermodynamic constraints, the CBM of the semiconductor must be located at a more negative level than the H^+/H_2 reduction potential

(0 V vs. SHE at pH 0), while the VBM should be more positive than the O_2/H_2O energy level (1.23 V vs. SHE at pH 0). Consequently, the theoretical minimum band gap energy required to drive water splitting is 1.23 eV. Nevertheless, considering the possible thermodynamic losses (0.4 eV) and overpotentials (0.3–0.4 eV), the practical minimum band gap energy of the semiconductor for this reaction should be around 1.9 eV [5, 61]. Generally, if one of these thermodynamic requirements is not fulfilled, no water splitting will take place. Therefore, using a semiconductor with suitable band positions is indispensable in this case.

To assess the water splitting performance of any photocatalytic system, the concept of solar to hydrogen efficiency (STH) is also often used together with the AQY evaluation. STH is defined as the product of the hydrogen production rate and the increase in Gibbs free energy (ΔG°) for the water splitting reaction divided by the total energy of incident solar irradiation:

$$\mathrm{STH} = \frac{\text{output energy}}{\text{incident solar light energy}} = \frac{r_{H_2} \times \Delta G^\circ}{P_{\text{sun}} \times S}, \tag{11}$$

where P_{sun} and S represent the flux energy of solar irradiation and the surface area of the system available for incident light, respectively. STH is considered as an absolute and practical standard to evaluate the water splitting performance of any photocatalyst under solar light irradiation [6]. An AM 1.5 G solar simulator (100 mW/cm^2) is commonly used as the source of solar light to evaluate STH.

In a recent review, it was estimated that for any photocatalytic water splitting system to compete with the conventional methane steam reforming process, it must attain STH of 10% and a lifetime exceeding 10 years [6, 10, 96]. Figure 2 shows the relationship between STH and available photon wavelength in an AM 1.5 G simulator at different AQYs [6]. For example, to achieve an STH of 10% when using solar irradiation with a wavelength of less than 600 nm, an AQY of 60% is needed. For UV utilization (<400 nm), the maximum possible STH is 1.7% even at an AQY of 100%. These calculations once again show the need to develop a photocatalytic system that can operate using a wider range of wavelengths of the solar spectrum.

3.1 Overall Water Splitting

To perform successful overall water splitting (OWS), there is a critical issue related to the rapid backward reaction (reformation of H_2O), which is thermodynamically predominant over the forward reaction. Consequently, deactivating the reverse reaction must be the top priority in designing any photocatalytic system for OWS [97]. One of the most popular methods of dealing with this problem is to apply a surface nanolayer coating [10]. This layer should be able to function as a molecular sieve, selectively allowing H_2 and water molecules to permeate through the layer while preventing O_2 molecules from diffusing and reaching the surface of the cocatalyst

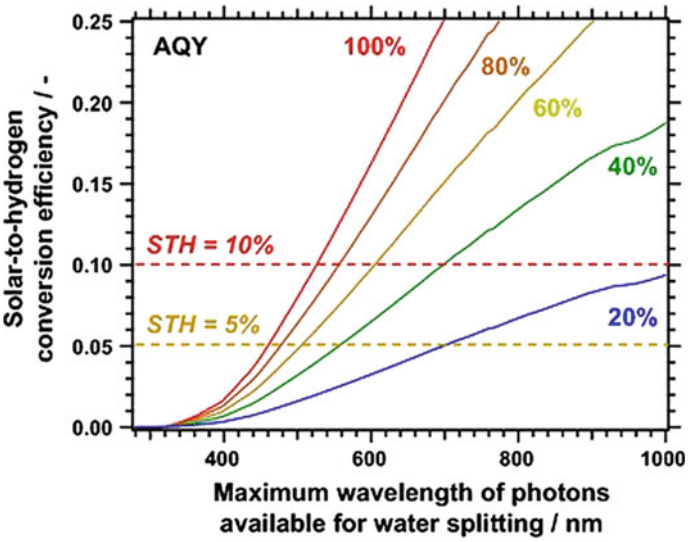

Fig. 2 Relationship between STH conversion efficiency and photon wavelength at different AQYs for photocatalytic water splitting. Reprinted with permission from Springer Science + Business Media New York: Springer US [6], Copyright (2014)

[98]. Since the reactive sites for backward and forward reactions are typically the same, this method effectively hinders the backward reaction. For example, a Cr_2O_3 nanolayer has been applied in many studies and found to be effective for inhibiting the reverse reaction, thus improving the photocatalytic OWS performance [22, 99]. The Cr_2O_3 nanolayer can be photodeposited on the surface of a cocatalyst by reducing the CrO_4^{2-} ions where it encapsulates the cocatalyst, thus producing a core–shell structure [99]. Figure 3 illustrates the mechanism by which the Cr_2O_3 nanolayer coating suppresses the backward reaction in photocatalytic OWS [100]. The Ni/NiO core/shell cocatalyst and hydrophilic nanolayers of amorphous oxyhydroxides of group IV and V transition metals (Ti, Nb, Zr, and Ta) are other successful examples of this technique [101, 102].

As mentioned earlier, a photocatalyst with suitable band positions is necessary to fulfill the thermodynamic requirement of any APS reaction. However, it is quite difficult to find a suitable semiconductor with CBM and VBM levels straddling the redox potentials of H^+/H_2 and O_2/H_2O. An appealing solution to this problem was demonstrated by Domen and his group, who used two semiconductors to form a two-step photoexcitation system, so-called Z-scheme water splitting (see Fig. 4), achieving STH exceeding 1% [22]. This method is inspired by natural photosynthesis, which also involves two photosystems where two different reactions occur separately as previously explained. Similarly, in the Z-scheme system, one semiconductor acts as a hydrogen evolution photocatalyst (HEP), while the other acts as an oxygen evolution photocatalyst (OEP). The remaining holes and electrons in the HEP and OEP respectively recombine through a solid-state electron mediator (e.g., Au, Rh, Ni,

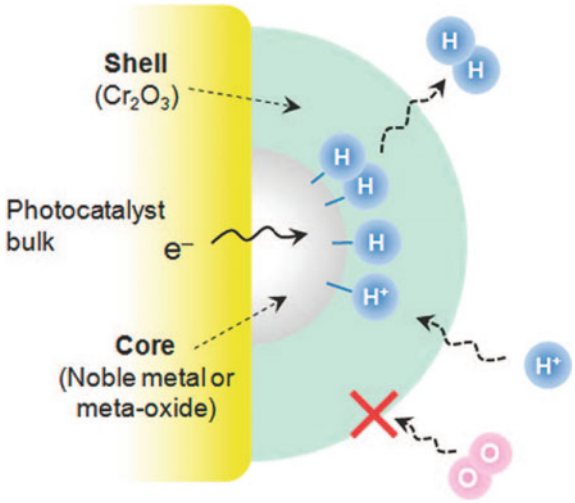

Fig. 3 Schematic illustration of the cocatalyst-Cr_2O_3 core–shell for suppressing the backward reaction in photocatalytic OWS. Reprinted with permission from Maeda and Domen, J. Phys. Chem. Lett., 1, 2,655–2,661 (2010) [100]. Copyright (2010) American Chemical Society

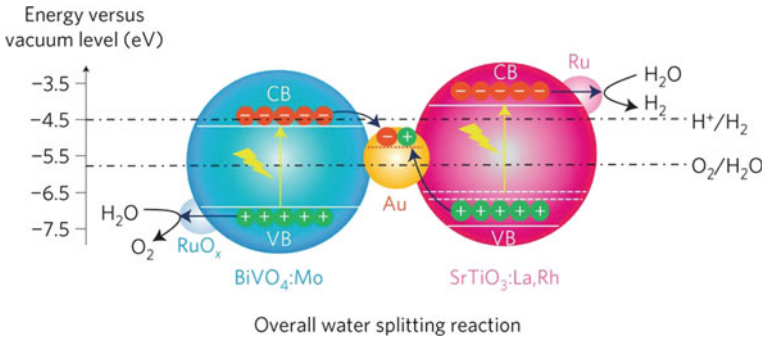

Fig. 4 Schematic of Z-scheme OWS on Ru-modified $SrTiO_3$:La,Rh/Au/$BiVO_4$:Mo particulate photocatalyst sheets. Reprinted with permission from Springer Nature [22], Copyright (2016)

Ag, Ir, and RGO) [22, 24, 103–105] or an aqueous redox mediator (e.g., Fe^{3+}/Fe^{2+} and IO_3^-/I^- solutions) [23, 106]. With this technique, semiconductors with unsuitable band positions (CBM lower than the H^+/H_2 redox potential or VBM higher than the O_2/H_2O potential) and a relatively small band gap can be utilized, thus expanding the choice of semiconductors [5, 9]. Furthermore, this system also provides a larger driving force for water splitting than the conventional photocatalytic system (one semiconductor) [10]. However, the major drawback of Z-scheme water splitting is the reduced amount of H_2 and O_2 produced, since half of the charge carriers recombine within the mediator [77].

3.2 Hydrogen Production from Sacrificial Water Splitting

Achieving OWS using a simple photocatalytic system is difficult in practice owing to many strict requirements that must be simultaneously satisfied [75]. Therefore, some researchers have attempted to apply a sacrificial agent as an irreversible electron donor or acceptor to perform an HER or OER separately, thus greatly reducing the complexity of the reaction. This sacrificial water splitting (SWS) method is relatively effective and efficient for assessing the suitability of a certain photocatalytic system for performing water splitting in terms of band positions, photogenerated charge dynamics, compatibility of the cocatalyst, and other properties [75]. Furthermore, since the reverse reaction (water formation) can be annulled in SWS, it is common to obtain a higher apparent production rate and quantum yield than in the case of OWS.

For HER, different semiconductors require different sacrificial agents (as an electron donor or hole scavenger) to obtain good performance. This phenomenon is due to the wide range of ability of semiconductors to oxidize a sacrificial agent [107]. For example, the semiconductor graphitic carbon nitride (g-C_3N_4) can exhibit superior performance when triethanolamine (TEOA) is used as a hole scavenger but has a rather poor performance when a different sacrificial agent is applied. Considering the cost and efficiency, the realization of this sacrificial photocatalytic hydrogen production strategy by utilizing biomass and abundant compounds in nature or industrial waste as the sacrificial agent will be of great significance [75].

CdS is an important and popular semiconductor which is often used in sacrificial HER. Although CdS has a very suitable band position for water splitting with a visible-light-responsive band gap (2.4 eV), it is ineffective for OWS owing to the self-photocorrosion phenomenon, which is often encountered with the use of sulfide materials [97]. The sulfur (S^{2-}) in CdS, instead of H_2O, is very susceptible to oxidation by photogenerated holes accompanied by the elution of the Cd^{2+} cation, as shown by the following equation [75]:

$$\mathrm{CdS} + 2h^+ \rightarrow \mathrm{Cd}^{2+} + \mathrm{S}. \tag{12}$$

Owing to this problem, a mixture of Na_2S and Na_2SO_3 is often utilized as a sacrificial agent, which not only protects the sulfide semiconductor from photocorrosion, thus producing a stable photocatalyst, but also greatly boosts its photocatalytic HER performance [48].

An interesting study about nature-inspired environmental phosphorylation to boost the sacrificial hydrogen production of g-C_3N_4 and several other semiconductors has been reported [62]. In NPS, phosphates play vital roles in establishing the Calvin cycle, acting as the transporter and pump for charge carrier transfer during light-dependent reactions and as mediators in carbon fixation during the dark reactions of photosynthesis. In this study, it was found that the addition of a phosphate component (KH_2PO_4) markedly boosted the H_2 generation of Pt/g-C_3N_4 by establishing a similar proton reduction mechanism to the one found in NPS (see Fig. 5),

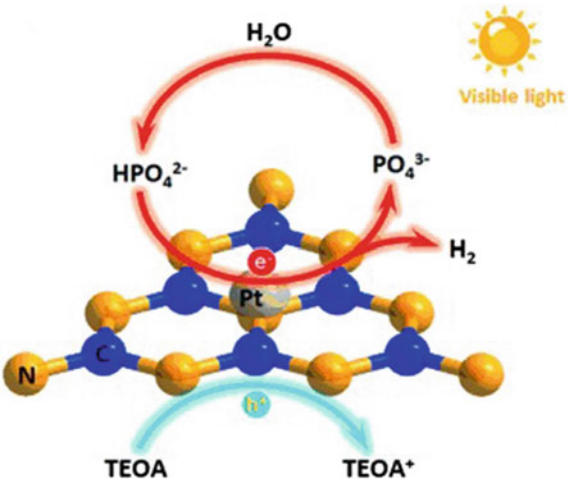

Fig. 5 Schematic illustration of photocatalytic H_2 evolution via the proton reduction mechanism involving HPO_4^{2-}. From Liu et al., Angew. Chem. Int. Ed., 54, 13,561–13,565 (2015) [62]. Copyright Wiley–VCH Verlag GmbH & Co. KGaA. Reproduced with permission

achieving a very high AQY of 26.1% at a wavelength of 420 nm for a g-C_3N_4-based photocatalyst. This finding may provide a promising and facile approach to highly efficient photocatalysis for both SWS and OWS in the future.

4 CO_2 Reduction

In modern society, owing to the rapidly increasing demand for energy, CO_2 emissions have escalated, resulting in a very serious state with NPS no longer compensating for CO_2 emission [108]. CO_2 is generally regarded as the main greenhouse gas, with excess CO_2 causing environmental problems, such as global warming, melting of the polar ice caps, sea level rises, and worsening droughts [108, 109]. These concerns have led to attempts to control the amount of CO_2 by converting CO_2 into harmless and useful chemical feedstocks [110]. Regarding this approach, solar-driven CO_2 conversion through APS is considered as one of the most reasonable and ideal approaches not only to reduce the imbalance between NPS and CO_2 emission, but also to provide a new type of energy feedstock, thus increasing the capacity of the global energy storage system [83, 111].

Since the carbon atom in CO_2 molecules possesses the highest valence, the photoreduction of CO_2 may result in a wide variety of carbon products with different oxidation states, ranging from gaseous CO and CH_4 to higher hydrocarbon species (e.g., C_2H_4, C_3H_8), as well as liquid-phase oxygenated hydrocarbons, such as CH_3OH and HCOOH (but not complex products such as carbohydrates) [112]. Table 2 shows the standard electrode potentials ($E°$) for the transformation of CO_2 into various products in aqueous media at pH 7 with respect to SHE. Unfortunately, CO_2 photoreduction is difficult to realize owing to the extreme stability of the CO_2

Table 2 Standard reduction potentials (pH 7) for the reactions of CO_2 reduction to different products in aqueous media

Reaction	E° versus SHE (V)
$CO_{2(g)} + e^- \rightarrow CO_2^-$	−1.90
$CO2_{(g)} + 2\ H^+_{(aq)} + 2\ e^- \rightarrow HCOOH_{(aq)}$	−0.61
$CO2_{(g)} + 2\ H^+_{(aq)} + 2\ e^- \rightarrow CO_{(g)} + H_2O_{(l)}$	−0.52
$CO2_{(g)} + 4\ H^+_{(aq)} + 4\ e^- \rightarrow HCHO_{(l)} + H_2O_{(l)}$	−0.48
$CO2_{(g)} + 6\ H^+_{(aq)} + 6\ e^- \rightarrow CH_3OH_{(l)} + H_2O_{(l)}$	−0.38
$CO2_{(g)} + 8\ H^+_{(aq)} + 8\ e^- \rightarrow CH_{4(g)} + H_2O_{(l)}$	−0.24
$2\ H^+_{(aq)} + 2\ e^- \rightarrow H_{2(g)}$	−0.41
$2\ H_2O_{(l)} \rightarrow O_{2(g)} + 4\ H^+_{(aq)} + 4\ e^-$	0.82

Source [83, 113]

molecule, ascribed to its two symmetric C = O bonds, which possess a high dissociation energy of about 750 kJ/mol [83]. In this case, the activation of CO_2 molecules very likely becomes the rate-determining step for the CO_2 reduction reaction [112]. Moreover, in the presence of water, CO_2 reduction must compete with proton reduction owing to the similar reduction potential and also the preferential adsorption of water compared with CO_2, thus resulting in the low selectivity and efficiency of the desired reaction [83].

From the kinetic perspective, the CO_2 reduction reaction is also challenging. The first step in CO_2 reduction is generally considered to be the formation of an intermediate CO_2^- (through a single electron transfer (ET) to a CO_2 molecule), whose reduction potential is very high (about −1.9 V) [112], as shown in Table 2. Consequently, a high overpotential is necessary[3] for the CO_2 reduction reaction to further proceed. Given this, an alternative reaction route involving a series of multiple proton-coupled electron transfer (PCET)[4] processes can be employed to bypass the formation of CO_2^-, thus avoiding the large activation barrier and the formation of unstable and high-energy intermediates [4, 83] (see Table 2). However, the PCET process is kinetically dependent on both the concentration of protons in the solution and the surface electron density at the reactive sites [112]. Moreover, since most of the CO_2 reduction products require multielectron transfer, the corresponding CO_2 reduction reactions are less kinetically favorable than the reduction of water, which only involves two electrons [112].

[3] Very few semiconductors have a CB level exceeding the $CO_2/\ CO_2^-$ reduction potential.

[4] In PCET, electron transfer is associated with proton (H^+) transfer. For the case of CO_2 reduction, the number of protons and electrons involved will also determine the products and reduction potential of the correponding reaction, as listed in Table 2.

In the following sections, we will briefly discuss the strategies for addressing some challenges in CO_2 reduction reactions: the activation of CO_2 molecules and controlling the selectivity of CO_2 reduction.

4.1 Activation of CO_2 Molecules

The activation of a CO_2 molecule is closely related to its adsorption by the surface atoms of a photocatalyst. The chemisorption of a CO_2 molecule induces the formation of a partially charged $CO_2^{\delta\bullet-}$ adsorbate, which no longer possesses a linear symmetrical structure [114]. The bending of CO_2 molecules is beneficial for lowering the barrier for electron transfer into CO_2 owing to the decrease in the lowest unoccupied molecular orbital (LUMO) level [114]. Hence, the basic strategy for driving the activation of CO_2 molecules is to promote the chemisorption of CO_2. Figure 6 shows some possible binding modes for the adsorption of a CO_2 molecule on the surface of a metal oxide (such as TiO_2), a popular photocatalyst for the photoreduction of CO_2 [115].

As approaches to activating CO_2 molecules, several practical strategies have been experimentally demonstrated, i.e., increasing the available surface area for adsorption, establishing surface defects, introducing surface basic sites, and employing a cocatalyst on the photocatalyst surface. In general, increasing the surface area of the photocatalyst, either by modifying the structure and morphology of the photocatalyst or by using a porous material, will provide more reactive sites for CO_2 adsorption [116–119]. Surface defects, such as oxygen vacancies [25, 79, 80] and sulfur vacancies [57–59], have attracted considerable attention in the last decade owing to their potential for generating an active trapping surface for CO_2 molecules. The challenge in this strategy is to prevent the formation of bulk defects, which usually occurs alongside the formation of surface defects, because bulk defects can act as recombination centers, which adversely affect the photocatalytic performance [75]. The formation of surface basic sites is also beneficial for CO_2 chemisorption owing to the Lewis acidity of the C atom, which enables CO_2 molecules to interact with the alkaline surface, thus leading to the formation of carbonate or bicarbonate intermediates [120–122]. Finally, a cocatalyst with a large work function, such as a noble metal, can also be employed, which may induce electron backdonation from metal d-orbitals into the (C–O) π^* orbital of CO_2, causing the formation of a $CO_2^{\delta\bullet-}$ adsorbate [109, 112].

It has also been reported that CO_2 molecules can be polarized and subsequently activated by utilizing highly energetic electrons excited by the localized surface plasmon resonance (LSPR) of some plasmonic nanometals (e.g., Au, Pt, Pd, etc.), assisted by thermal energy [123–127]. The LSPR effect is defined as the resonant photon-induced collective oscillation of valence electrons, established when the frequency of the photons matches the natural frequency of the surface electrons oscillating against the restoring force of positive nuclei [128]. This phenomenon generates hot electrons with very high energy, which are very effective for disrupting

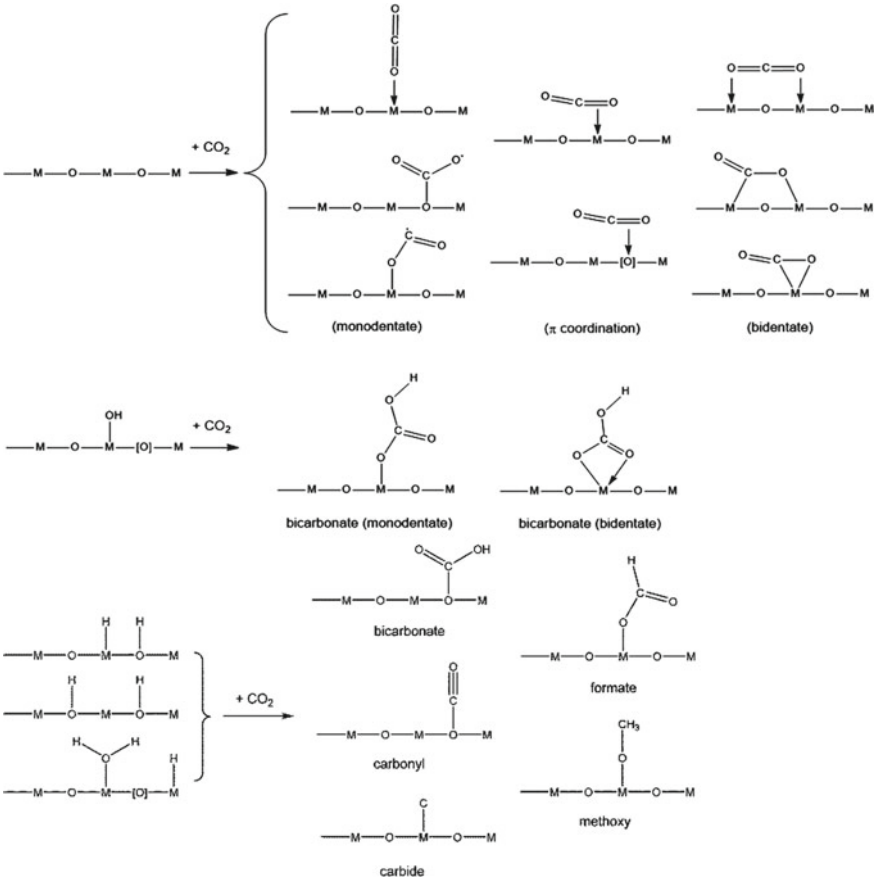

Fig. 6 Modes of adsorption for CO_2 on the surfaces of regular and modified metal oxides. Reproduced from Ref. [115] with permission from The Royal Society of Chemistry

the stability of CO_2 molecules [129]. Figure 7 illustrates a schematic and the reaction mechanism of the LSPR effect over a Pt-Au/SiO_2 catalyst for the photoreduction of CO_2 [127]. Following these studies, the photothermal effect through the self-heating process was observed on an illuminated boron catalyst[5] [130]. It is well known that CO_2 molecules are more reactive at high temperatures. In this case, the photothermal effect of boron can induce a high local temperature, which facilitates CO_2 activation. It also triggers the self-hydrolysis of boron particles, which in situ produces H_2 as the active proton source and electron donor for CO_2 reduction, as well as boron oxides that function as promoters of CO_2 adsorption onto the surface of boron catalysts. All these effects synergistically promote the CO_2 reduction reaction.

[5] The corresponding photothermal process is actually considerably different from the conventional APS process, which involves the generation of charge carriers. However, since this effect is entirely driven by the illumination of light, we decided to include this study in the discussion.

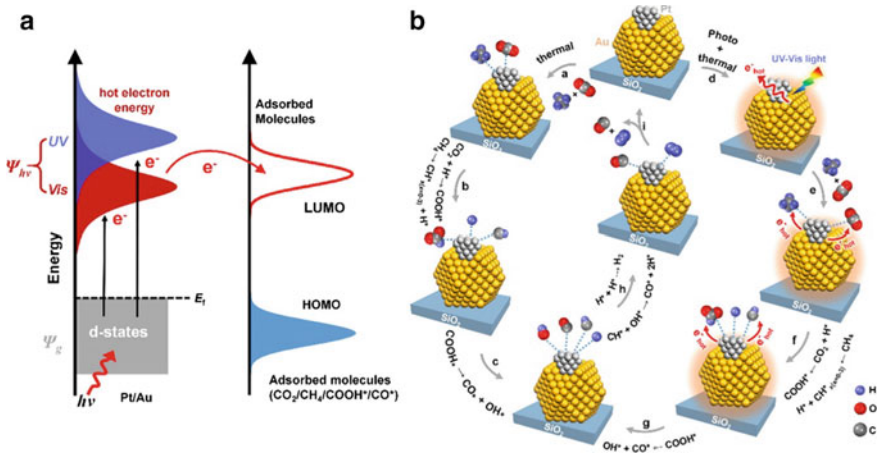

Fig. 7 **a** Schematic of LSPR effect generating light-excited hot electrons for the activation of stable compounds, such as CO_2 and CH_4. **b** Proposed reaction mechanism for photocatalytic CO_2 reduction over Pt-Au/SiO_2 by utilizing the dry reforming of methane (DRM) reaction. Reprinted with permission from Song et al., ACS Appl. Mater. Interfaces, 10, 408–416 (2018) [127]. Copyright (2018) American Chemical Society

4.2 Controlling the Selectivity of CO_2 Reduction

As mentioned earlier, CO_2 reduction has several possible reaction pathways, depending on the number of electrons involved in the reactions, leading to various carbon products. Therefore, in addition to the competition with proton reduction, it is also important to ensure that the CO_2 reduction selectively proceeds through the desired reaction. In short, the binding mode of CO_2 during the adsorption state (see Fig. 6) determines the route that the reaction takes [112, 115]. Accordingly, tuning the surface features of the photocatalyst to favor the formation of a particular adsorbate intermediate, which in turn will be converted into the desired carbon product, is the key to controlling the selectivity of CO_2 reduction.

The cocatalyst is also important for not only kinetically driving the multielectron reaction of CO_2 reduction (since it may serve as an electron-trapping center), but also tuning the selectivity of the reaction [109]. The final product of the reaction may vary with the adsorption properties of the intermediate, electron transfer (for proton reduction and CO_2 activation) overpotentials, loading method, elemental composition, dispersion, particle size, structure, and exposed sites of the cocatalyst [109, 112, 131]. Therefore, the careful selection and design of the cocatalyst are indispensable for regulating the reaction mechanism [109]. Figure 8 summarizes the general selectivity trends of CO_2 reduction over various metal-based cathodes [132]. In addition, it is also necessary to tune the experimental conditions. Among the many experimental parameters, the pH of the solution can considerably affect the CO_2 reduction reaction mechanism [131]. pH not only determines the concentration

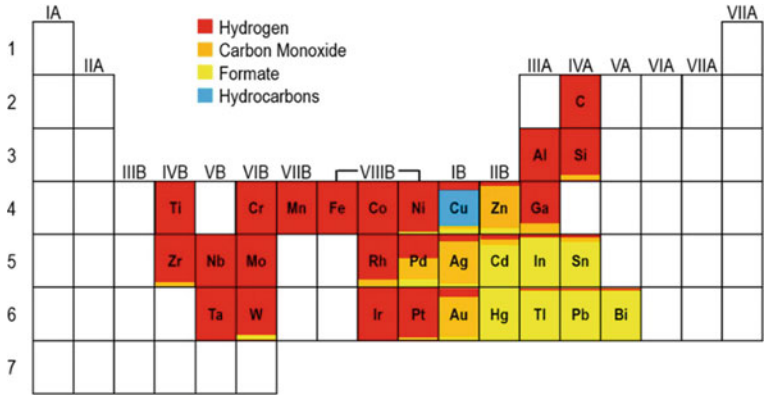

Fig. 8 Section of the periodic table depicting the primary products in CO_2 reduction over some metal-based electrodes. Reprinted with permission from White et al., Chem. Rev., 115, 12,888–12,935 (2015) [132]. Copyright (2015) American Chemical Society

of H^+ ions in the solution (which is related to the rate of H_2 evolution), but also affects the solubility of CO_2 and the relative concentrations of CO_3^{2-} and HCO_3^-, which are strongly correlated with the modes of CO_2 adsorption [112, 131].

5 N_2 Fixation

The N_2 fixation reaction can be regarded as one of the most crucial chemical processes in nature, considering the importance of fixed nitrogen compounds[6] for living organisms on this planet, owing to its integral role in producing basic biological building blocks [85, 133, 134]. In particular, ammonia (NH_3), the main product of N_2 fixation, is a very important raw material for the production of fertilizers and also as a promising carbon-free energy carrier [135–137]. The first work on photocatalytic nitrogen fixation in sterile soils containing natural abundant oxides was performed by Dhar and Pant in the early 1940s [138]. Subsequently, around 30–40 years later, Schrauzer and Guth provided more thorough reports of photon-driven nitrogen fixation over natural materials and as-synthesized TiO_2 [19, 139]. These early studies triggered numerous extensive works to investigate nitrogen fixation over some well-designed synthetic photocatalysts [133]. Unfortunately, in the following decades, the studies on semiconductor-based photocatalytic nitrogen fixation were considerably hindered (as indicated by the substantially fewer reported studies) by the difficulties in N_2 adsorption and activation over the catalytic surface, which were a stumbling block to further development and achieving competitive performance with other methods [133, 136, 137]. Nevertheless, owing to the recent advancement

[6] They are identified by their lack of N–N bonds and can take both the oxidized and reduced forms of N_2, such as NH_3, nitrogen oxides, nitrates, and urea [133].

of nanotechnologies and nanomaterials, which can provide solutions to such kinetic limitations, photocatalytic N_2 fixation has returned to the main stage in the field of APS in the past few years [85].

Being the 'youngest' of the APS applications, photon-driven N_2 fixation still has a long way to go before an ideal catalytic N_2 photofixation system can be devised, inasmuch as the comprehensive knowledge and understanding of the mechanistic principles of the reaction and also suitable materials are still lacking [85]. In this section, we briefly discuss the basic mechanism of N_2 photofixation (especially to NH_3), the requirements and challenges in achieving effective reaction processes, and the possible approaches to deal with them. The discussion herein is expected to contribute to filling the knowledge gap in the study of APS-based N_2 fixation.

5.1 Fundamentals of Photon-Driven N_2 Fixation

The N_2 fixation and CO_2 reduction reactions actually have many things in common. Similar to the CO_2 molecule, the N_2 molecule is also very stable owing to its extremely strong N≡N bond, with a dissociation energy of 945 kJ/mol for the direct cleavage of the triple bond [85]. As a result, a single ET (−4.16 V vs. SHE) and PCET (−3.20 V vs. SHE) to the N_2 molecule (for its activation) are almost thermodynamically imposible with currently available semiconductors owing to their very high reduction potentials. Therefore, in a similar way to the CO_2 reduction reaction mechanism, multiple PCET processes can also be applied in the N_2 reduction reaction to avoid the principal energy barrier while bypassing the formation of high-energy intermediates [140, 141]. Multiple PCET, depending on the number of protons and electrons involved, may lead to various partially reduced and stable intermediate species (e.g., N_2H_2 and N_2H_4) other than NH_3, thus resulting in competition between them and also with the water reduction reaction [140]. Table 3 provides

Table 3 Standard reduction potentials (pH 0) for the reactions of N_2 reduction to NH_3 in aqueous media

Reaction	$E°$ versus SHE (V)
$N_{2(g)} + e^- \rightarrow {N_2}^-{}_{(aq)}$	−4.16
$N_{2(g)} + {H^+}_{(aq)} + e^- \rightarrow N_2H_{(g)}$	−3.20
$N_{2(g)} + 2\ {H^+}_{(aq)} + 2\ e^- \rightarrow N_2H_{2(g)}$	−1.20
$N_{2(g)} + 4\ {H^+}_{(aq)} + 4\ e^- \rightarrow N_2H_{4(g)}$	−0.33
$N_{2(g)} + 5\ {H^+}_{(aq)} + 4\ e^- \rightarrow {N_2H_5}^+{}_{(aq)}$	−0.23
$N2_{(g)} + 6\ {H^+}_{(aq)} + 6\ e^- \rightarrow 2\ NH_{3(g)}$	0.09
$N2_{(g)} + 8\ {H^+}_{(aq)} + 6\ e^- \rightarrow 2\ {NH_4}^+{}_{(aq)}$	0.27
$2\ {H^+}_{(aq)} + 2\ e^- \rightarrow H_{2(g)}$	0.00
$2\ H_2O_{(l)} \rightarrow O_{2(g)} + 4\ {H^+}_{(aq)} + 4\ e^-$	1.23

Source [140, 141, 143]

a list of possible N_2 reduction reactions in aqueous media and their corresponding standard reduction potentials.

The extremely high stability of the N_2 molecule is also a major disadvantage regarding the kinetic feasibility of the N_2 fixation reaction. Because of the high stability, the adsorption and activation of the N_2 molecule can be considered as the rate-limiting steps of the overall reaction [142]. For the same reason, it still remains a major challenge to enhance the kinetic feasibility of the N_2 photofixation reaction. Therefore, even though there are other concerns that must be looked into and dealt with carefully, in the next section, we will only discuss the adsorption and activation of N_2, the most crucial yet challenging steps in the N_2 fixation reaction.

5.2 Adsorption and Activation of N_2 Molecules

Similar to the CO_2 molecule, the activation of the N_2 molecule is also strongly associated with the adsorption of the species on the catalytic surface, since electron transfer can only occur when there is an intimate interaction between the chemical species and the catalyst [142]. Generally, a photocatalyst with a high surface area is favorable for heterogeneous catalytic reactions, including N_2 fixation, owing to its capability of adsorbing more reactants [144]. Some other potential approaches for promoting the adsorption of N_2 molecules by employing surface defects, such as nitrogen vacancies [69, 145] and oxygen vacancies [74, 146], have been succesfully demonstrated for various nitride and oxide semiconductors, respectively. The vacancy species on the surface of a semiconductor can be occupied by N atoms, thus enabling swift electron donation to the adsorbed N_2 owing to the direct contact between the photocatalyst and the N_2 molecules. Such a phenomenon is essential for the N_2 activation step and will be discussed later. To suppress the faster H_2 reduction reaction, employing a metal-based catalyst with stronger adsorption of N atoms than that of H atoms might be a promising strategy worth investigating and exploring more thoroughly [147, 148].

Regarding N_2 activation, it is beneficial for the adsorbing sites to be able to synergically accept electrons from and backdonate to N_2, which simultaneously weakens the N_2 bond[7] and strengthens the bond between the sites and N_2, as illustrated in Fig. 9 [135]. As a result, the adsorbed N_2 is more susceptible to electron donation owing to the reduced resistance and activation energy barrier of the attenuated N_2 bond. Subsequently promoting charge exchange between the catalyst and N_2 is essential to provide an accessible kinetic pathway towards the activation step and later stages of the reaction [85]. Interestingly, the above-mentioned strategies can be simultaneously employed by generating vacancy species on the surface of a semiconductor, which is a powerful method of promoting the photocatalytic N_2 fixation reaction, as mentioned earlier, owing to the N_2-capturing ability and nature of the vacancy as an

[7] The weakening of the N_2 bond is usually associated with an increase in its bond length, indicating a lower bond energy.

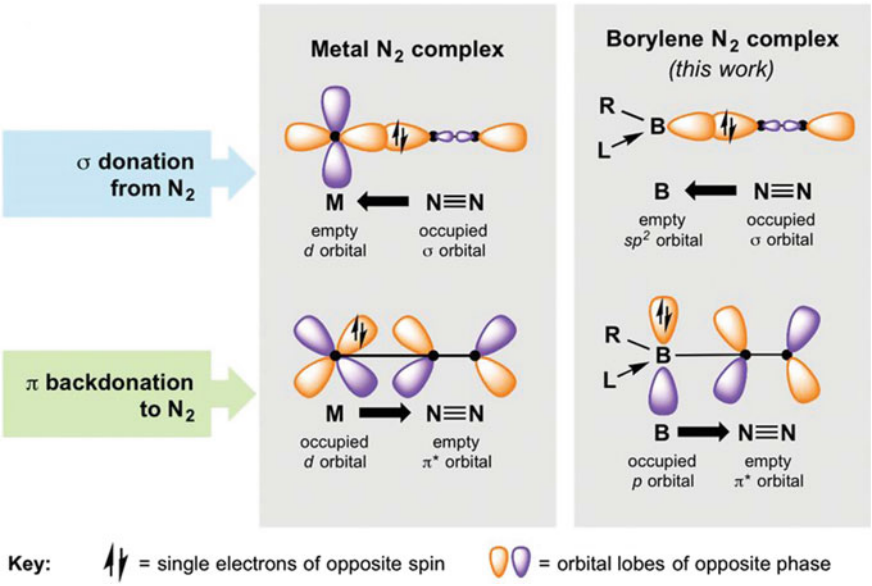

Fig. 9 Simplified schematic of bonding in well-known end-on bound transition metal N_2 complexes (left) and monovalent boron species (right). From Légaré et al., Science, 359, 896–900 (2018) [135]. Reprinted with permission from AAAS

electron localization center [74]. When the surface vacancy successfully binds a N_2 molecule, the backtransfer of charges from the vacancy to the adsorbed N_2 occurs, rendering electron depletion on the vacancy and electron accumulation on the N_2 molecule [71].

Even though a vacancy possesses great potential for N_2 adsorption and activation, a surface vacancy can be easily consumed through oxidation or a similar phenomenon, leading to the deactivation of the photocatalyst [149]. Vacancy stabilization through the self-regeneration of the vacancy under light irradiation is therefore an ideal solution to this problem [74, 149]. Very recently, an excellent example of light-switchable oxygen vacancy circulation for sustainable N_2 fixation on an ultrafine Bi_5O_7Br nanotube has been reported, the scheme of which is shown in Fig. 10 [74]. In addition, similar to the CO_2 molecule, the N_2 molecule can also be activated by utilizing hot electrons produced through the LSPR effect [26, 27, 150].

6 Summary and Outlook

Owing to the rapid advancement of human civilization, both global energy consumption and environmental pollution have increased significantly and almost uncontrollably. To make matters worse, the regeneration of fossil fuels, our current primary

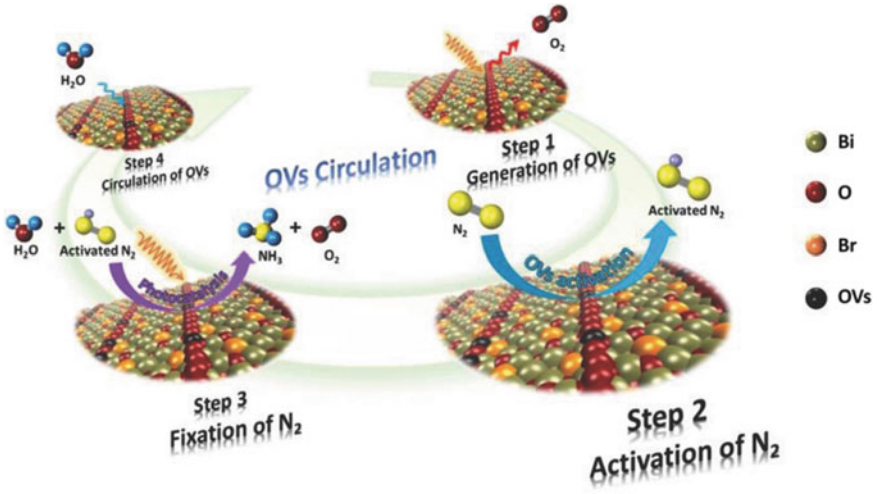

Fig. 10 Schematic illustration of photoinduced oxygen vacancy (OV) circulation for N_2 fixation on Bi_5O_7Br. From Wang et al., Adv. Mater. 29, 1,701,774 (2017) [74]. Copyright Wiley–VCH Verlag GmbH & Co. KGaA. Reproduced with permission

energy resource, is extremely slow. Thus, the realization of artifical photosynthesis (APS) technology to exploit and convert the limitless solar energy into renewable, clean, and sustainable energy feedstocks has become an urgent task requiring intensive and extensive effort and study. For this reason, many APS-based scientists and researchers have attempted to acquire in-depth and comprehensive knowledge on the APS reaction mechanism as well as practical and efficient approaches to devise an ideal photocatalytic system.

In this chapter, we have summarized the basic concepts in designing an effective photocatalytic system by examining the general steps in the APS process, i.e., photon absorption, charge carrier migration, and the surface reaction. Furthermore, the fundamentals of three important APS reactions (water splitting, CO_2 reduction, and N_2 fixation) as well as the specific challenges of each reaction and some possible strategies to address them were briefly introduced. We also discussed several effective strategies for improving the performance of some photocatalytic materials in diverse applications, such as a surface nanolayer coating, the Z-scheme system, the sacrificial photocatalytic reaction, the localized surface plasmon resonance (LSPR) phenomenon, and surface defects (self-regeneration).

While considerable advances in APS research have recently been accomplished, efficiency, stability, and cost are still the main issues that must be simultaneously overcome to enable APS technology to enter industrial use. The development of novel photocatalytic materials, either by modifying currently available materials or by discovering completely new materials, may lead to a significant breakthrough in these problems. Correspondingly, surface and interface engineering are indispensable for the fabrication of outstanding materials with distinctive and useful features, and

thus should be considered and further extended. Last but not least, it is also important to carry out an in-depth study of the mechanism through the combination of in situ observation and a theoretical approach (commonly by computational methods) to obtain a full, accurate, and detailed understanding of the mechanism behind all APS processes.

References

1. Bard AJ, Fox MA (1995) Artificial photosynthesis: solar splitting of water to hydrogen and oxygen. Acc Chem Res 28(3):141–145. https://doi.org/10.1021/ar00051a007
2. Benniston AC, Harriman A (2008) Artificial Photosynthesis. Mater Today 11(12):26–34. https://doi.org/10.1016/S1369-7021(08)70250-5
3. Balzani V, Credi A, Venturi M (2008) Photochemical conversion of solar energy. Chemsuschem 1(1–2):26–58. https://doi.org/10.1002/cssc.200700087
4. Lewis NS, Nocera DG (2006) Powering the planet: chemical challenges in solar energy utilization. Proc Natl Acad Sci U.S.A. 103(43):15729–15735. https://doi.org/10.1073/pnas.0603395103
5. Tachibana Y, Vayssieres L, Durrant JR (2012) Artificial photosynthesis for solar water-splitting. Nat. Photonics 6:511–518. https://doi.org/10.1038/nphoton.2012.175
6. Hisatomi T, Takanabe K, Domen K (2015) Photocatalytic water-splitting reaction from catalytic and kinetic perspectives. Catal Lett 145(1):95–108. https://doi.org/10.1007/s10562-014-1397-z
7. Zhu S, Wang D (2017) Photocatalysis: basic principles, diverse forms of implementations and emerging scientific opportunities. Adv Energy Mater 7(23):1700841. https://doi.org/10.1002/aenm.201700841
8. Zhang J, Hu S, Wang Y (2014) A convenient method to prepare a novel alkali metal sodium doped carbon nitride photocatalyst with a tunable band structure. RSC Adv 4(108):62912–62919. https://doi.org/10.1039/C4RA11377B
9. Wang Y, Suzuki H, Xie J, Tomita O, Martin DJ, Higashi M, Kong D, Abe R, Tang J (2018) Mimicking natural photosynthesis: solar to renewable H_2 fuel synthesis by Z-scheme water splitting systems. Chem Rev 118(10):5201–5241. https://doi.org/10.1021/acs.chemrev.7b00286
10. Chen S, Takata T, Domen K (2017) Particulate photocatalysts for overall water splitting. Nat Rev Mater 2:17050. https://doi.org/10.1038/natrevmats.2017.50
11. Maeda K, Domen K (2007) New non-oxide photocatalysts designed for overall water splitting under visible light. J Phys Chem C 111(22):7851–7861. https://doi.org/10.1021/jp070911w
12. Fujishima A, Honda K (1972) Electrochemical photolysis of water at a semiconductor electrode. Nature 238:37–38. https://doi.org/10.1038/238037a0
13. Slamet R, Gunlazuardi J, Dewi EL (2017) Enhanced photocatalytic activity of Pt deposited on titania nanotube arrays for the hydrogen production with glycerol as a sacrificial agent. Int J Hydrogen Energy 42(38):24014–24025. https://doi.org/10.1016/j.ijhydene.2017.07.208
14. Slamet TD, Valentina IM (2013) Photocatalytic hydrogen production from glycerol-water mixture over Pt-N-TiO_2 nanotube photocatalyst. Int J Energy Res 37(11):1372–1381. https://doi.org/10.1002/er.2939
15. de Brito JF, Tavella F, Genovese C, Ampelli C, Zanoni MVB, Centi G, Perathoner S (2018) Role of CuO in the modification of the photocatalytic water splitting behavior of TiO_2 nanotube thin films. Appl Catal B: Environ 224:136–145. https://doi.org/10.1016/j.apcatb.2017.09.071

16. Tan L-L, Ong W-J, Chai S-P, Mohamed AR (2015) Noble metal modified reduced graphene Oxide/TiO_2 ternary nanostructures for efficient visible-light-driven photoreduction of carbon dioxide into methane. Appl Catal B: Environ 166–167:251–259. https://doi.org/10.1016/j.apcatb.2014.11.035
17. Varghese OK, Paulose M, LaTempa TJ, Grimes CA (2009) High-rate solar photocatalytic conversion of CO_2 and water vapor to hydrocarbon fuels. Nano Lett 9(2):731–737. https://doi.org/10.1021/nl803258p
18. Ye M, Wang X, Liu E, Ye J, Wang D (2018) Boosting the photocatalytic activity of P25 for carbon dioxide reduction by using a surface-alkalinized titanium carbide MXene as cocatalyst. Chemsuschem 11(10):1606–1611. https://doi.org/10.1002/cssc.201800083
19. Schrauzer GN, Guth TD (1977) Photolysis of water and photoreduction of nitrogen on titanium dioxide. J Am Chem Soc 99(22):7189–7193. https://doi.org/10.1021/ja00464a015
20. Hirakawa H, Hashimoto M, Shiraishi Y, Hirai T (2017) Photocatalytic conversion of nitrogen to ammonia with water on surface oxygen vacancies of titanium dioxide. J Am Chem Soc 139(31):10929–10936. https://doi.org/10.1021/jacs.7b06634
21. Zhao W, Zhang J, Zhu X, Zhang M, Tang J, Tan M, Wang Y (2014) Enhanced nitrogen photofixation on Fe-doped TiO_2 with highly exposed (101) facets in the presence of ethanol as scavenger. Appl Catal B: Environ 144:468–477. https://doi.org/10.1016/j.apcatb.2013.07.047
22. Wang Q, Hisatomi T, Jia Q, Tokudome H, Zhong M, Wang C, Pan Z, Takata T, Nakabayashi M, Shibata N, Li Y, Sharp ID, Kudo A, Yamada T, Domen K (2016) Scalable water splitting on particulate photocatalyst sheets with a solar-to-hydrogen energy conversion efficiency exceeding 1%. Nat Mater 15:611–615. https://doi.org/10.1038/nmat4589
23. Kato H, Sasaki Y, Shirakura N, Kudo A (2013) Synthesis of highly active rhodium-doped $SrTiO_3$ powders in Z-scheme systems for visible-light-driven photocatalytic overall water splitting. J Mater Chem A 1(39):12327–12333. https://doi.org/10.1039/C3TA12803B
24. Wang Q, Li Y, Hisatomi T, Nakabayashi M, Shibata N, Kubota J, Domen K (2015) Z-scheme water splitting using particulate semiconductors immobilized onto metal layers for efficient electron relay. J Catal 328:308–315. https://doi.org/10.1016/j.jcat.2014.12.006
25. Xie K, Umezawa N, Zhang N, Reunchan P, Zhang Y, Ye J (2011) Self-doped $SrTiO_{3-\delta}$ photocatalyst with enhanced activity for artificial photosynthesis under visible light. Energy Environ Sci 4(10):4211–4219. https://doi.org/10.1039/C1EE01594J
26. Oshikiri T, Ueno K, Misawa H (2014) Plasmon-induced ammonia synthesis through nitrogen photofixation with visible light irradiation. Angew Chem Int Ed 53(37):9802–9805. https://doi.org/10.1002/anie.201404748
27. Oshikiri T, Ueno K, Misawa H (2016) Selective dinitrogen conversion to ammonia using water and visible light through plasmon-induced charge separation. Angew Chem Int Ed 55(12):3942–3946. https://doi.org/10.1002/anie.201511189
28. Ohno T, Bai L, Hisatomi T, Maeda K, Domen K (2012) Photocatalytic water splitting using modified GaN:ZnO solid solution under visible light: long-time operation and regeneration of activity. J Am Chem Soc 134(19):8254–8259. https://doi.org/10.1021/ja302479f
29. Yang X, Wolcott A, Wang G, Sobo A, Fitzmorris RC, Qian F, Zhang JZ, Li Y (2009) Nitrogen-doped ZnO nanowire arrays for photoelectrochemical water splitting. Nano Lett 9(6):2331–2336. https://doi.org/10.1021/nl900772q
30. Xin C, Hu M, Wang K, Wang X (2017) Significant enhancement of photocatalytic reduction of CO_2 with H_2O over ZnO by the formation of basic zinc carbonate. Langmuir 33(27):6667–6676. https://doi.org/10.1021/acs.langmuir.7b00620
31. Zhang S, Yin X, Zheng Y (2018) Enhanced photocatalytic reduction of CO_2 to methanol by ZnO nanoparticles deposited on ZnSe nanosheet. Chem Phys Lett 693:170–175. https://doi.org/10.1016/j.cplett.2018.01.018

32. Zhang X, Wang X, Wang D, Ye J (2019) Conformal $BiVO_4$-layer/WO_3-nanoplate-array heterojunction photoanode modified with cobalt phosphate cocatalyst for significantly enhanced photoelectrochemical performances. ACS Appl Mater Interfaces 11(6):5623–5631. https://doi.org/10.1021/acsami.8b05477
33. Pihosh Y, Turkevych I, Mawatari K, Asai T, Hisatomi T, Uemura J, Tosa M, Shimamura K, Kubota J, Domen K, Kitamori T (2014) Nanostructured WO_3/$BiVO_4$ photoanodes for efficient photoelectrochemical water splitting. Small 10(18):3692–3699. https://doi.org/10.1002/smll.201400276
34. Gao S, Gu B, Jiao X, Sun Y, Zu X, Yang F, Zhu W, Wang C, Feng Z, Ye B, Xie Y (2017) Highly efficient and exceptionally durable CO_2 photoreduction to methanol over freestanding defective single-unit-cell bismuth vanadate layers. J Am Chem Soc 139(9):3438–3445. https://doi.org/10.1021/jacs.6b11263
35. Dias P, Lopes T, Meda L, Andrade L, Mendes A (2016) Photoelectrochemical water splitting using WO_3 photoanodes: the substrate and temperature roles. PCCP 18(7):5232–5243. https://doi.org/10.1039/C5CP06851G
36. Chen X, Zhou Y, Liu Q, Li Z, Liu J, Zou Z (2012) Ultrathin, single-crystal WO_3 nanosheets by two-dimensional oriented attachment toward enhanced photocatalystic reduction of CO_2 into hydrocarbon fuels under visible light. ACS Appl Mater Interfaces 4(7):3372–3377. https://doi.org/10.1021/am300661s
37. Wang P-Q, Bai Y, Luo P-Y, Liu J-Y (2013) Graphene–WO_3 nanobelt composite: elevated conduction band toward photocatalytic reduction of CO_2 into hydrocarbon fuels. Catal Commun 38:82–85. https://doi.org/10.1016/j.catcom.2013.04.020
38. Wang D, Pierre A, Kibria MG, Cui K, Han X, Bevan KH, Guo H, Paradis S, Hakima A-R, Mi Z (2011) Wafer-level photocatalytic water splitting on GaN nanowire arrays grown by molecular beam epitaxy. Nano Lett 11(6):2353–2357. https://doi.org/10.1021/nl2006802
39. AlOtaibi B, Fan S, Wang D, Ye J, Mi Z (2015) Wafer-level artificial photosynthesis for CO_2 reduction into CH_4 and CO using GaN nanowires. ACS Catal 5(9):5342–5348. https://doi.org/10.1021/acscatal.5b00776
40. Standing A, Assali S, Gao L, Verheijen MA, van Dam D, Cui Y, Notten PHL, Haverkort JEM, Bakkers EPAM (2015) Efficient water reduction with gallium phosphide nanowires. Nat Commun 6:7824. https://doi.org/10.1038/ncomms8824
41. Sun J, Liu C, Yang P (2011) Surfactant-free, large-scale, solution–liquid–solid growth of gallium phosphide nanowires and their use for visible-light-driven hydrogen production from water reduction. J Am Chem Soc 133(48):19306–19309. https://doi.org/10.1021/ja2083398
42. Barton EE, Rampulla DM, Bocarsly AB (2008) Selective solar-driven reduction of CO_2 to methanol using a catalyzed p-GaP based photoelectrochemical Cell. J Am Chem Soc 130(20):6342–6344. https://doi.org/10.1021/ja0776327
43. Zeng G, Qiu J, Li Z, Pavaskar P, Cronin SB (2014) CO_2 reduction to methanol on TiO_2-passivated GaP photocatalysts. ACS Catal 4(10):3512–3516. https://doi.org/10.1021/cs500697w
44. Maeda K, Lu D, Domen K (2013) Direct water splitting into hydrogen and oxygen under visible light by using modified TaON photocatalysts with d^0 electronic configuration. Chem Eur J 19(16):4986–4991. https://doi.org/10.1002/chem.201300158
45. Ma SSK, Maeda K, Domen K (2012) Modification of TaON with ZrO_2 to improve photocatalytic hydrogen evolution activity under visible light: influence of preparation conditions on activity. Catal Sci Technol 2(4):818–823. https://doi.org/10.1039/C2CY00499B
46. Hara M, Kondo T, Komoda M, Ikeda S, Kondo JN, Domen K, Hara M, Shinohara K, Tanaka A (1998) Cu_2O as a photocatalyst for overall water splitting under visible light irradiation. Chem Commun 3:357–358. https://doi.org/10.1039/A707440I
47. Zhao Y, Wang W, Li Y, Zhang Y, Yan Z, Huo Z (2014) Hierarchical branched Cu_2O nanowires with enhanced photocatalytic activity and stability for H_2 production. Nanoscale 6(1):195–198. https://doi.org/10.1039/C3NR04280D

48. Chang K, Li M, Wang T, Ouyang S, Li P, Liu L, Ye J (2015) Drastic layer-number-dependent activity enhancement in photocatalytic H_2 evolution over $nMoS_2/CdS$ ($n \geq 1$) under visible light. Adv Energy Mater 5(10):1402279. https://doi.org/10.1002/aenm.201402279
49. Hai X, Zhou W, Wang S, Pang H, Chang K, Ichihara F, Ye J (2017) Rational design of freestanding MoS_2 monolayers for hydrogen evolution reaction. Nano Energy 39:409–417. https://doi.org/10.1016/j.nanoen.2017.07.021
50. Zhao G, Sun Y, Zhou W, Wang X, Chang K, Liu G, Liu H, Kako T, Ye J (2017) Superior photocatalytic H_2 production with cocatalytic Co/Ni species anchored on sulfide semiconductor. Adv Mater 29(40):1703258. https://doi.org/10.1002/adma.201703258
51. Zhao G, Zhou W, Sun Y, Wang X, Liu H, Meng X, Chang K, Ye J (2018) Efficient photocatalytic CO_2 reduction over Co(II) species modified CdS in aqueous solution. Appl Catal B: Environ 226:252–257. https://doi.org/10.1016/j.apcatb.2017.12.054
52. Jin J, Yu J, Guo D, Cui C, Ho W (2015) A hierarchical Z-scheme CdS–WO_3 photocatalyst with enhanced CO_2 reduction activity. Small 11(39):5262–5271. https://doi.org/10.1002/smll.201500926
53. Khan MMT, Bhardwaj RC, Bhardwaj C (1988) Catalytic fixation of nitrogen by the photocatalytic CdS/Pt/RuO_2 particulate system in the presence of aqueous $[Ru(Hedta)N_2]^{\ominus}$ complex. Angew Chem Int Ed Engl 27(7):923–925. https://doi.org/10.1002/anie.198809231
54. Brown KA, Harris DF, Wilker MB, Rasmussen A, Khadka N, Hamby H, Keable S, Dukovic G, Peters JW, Seefeldt LC, King PW (2016) Light-driven dinitrogen reduction catalyzed by a CdS: nitrogenase MoFe protein biohybrid. Science 352(6284):448–450. https://doi.org/10.1126/science.aaf2091
55. Zhang J, Yu J, Zhang Y, Li Q, Gong JR (2011) Visible light photocatalytic H_2-production activity of CuS/ZnS porous nanosheets based on photoinduced interfacial charge transfer. Nano Lett 11(11):4774–4779. https://doi.org/10.1021/nl202587b
56. Tsuji I, Kudo A (2003) H_2 evolution from aqueous sulfite solutions under visible-light irradiation over Pb and halogen-codoped ZnS photocatalysts. J Photochem Photobiol A 156(1):249–252. https://doi.org/10.1016/S1010-6030(02)00433-1
57. Meng X, Yu Q, Liu G, Shi L, Zhao G, Liu H, Li P, Chang K, Kako T, Ye J (2017) Efficient photocatalytic CO_2 reduction in all-inorganic aqueous environment: cooperation between reaction medium and Cd(II) modified colloidal ZnS. Nano Energy 34:524–532. https://doi.org/10.1016/j.nanoen.2017.03.021
58. Meng X, Zuo G, Zong P, Pang H, Ren J, Zeng X, Liu S, Shen Y, Zhou W, Ye J (2018) A rapidly room-temperature-synthesized Cd/ZnS: Cu nanocrystal photocatalyst for highly efficient solar-light-powered C_O2 reduction. Appl Catal B: Environ 237:68–73. https://doi.org/10.1016/j.apcatb.2018.05.066
59. Pang H, Meng X, Song H, Zhou W, Yang G, Zhang H, Izumi Y, Takei T, Jewasuwan W, Fukata N, Ye J (2019) Probing the role of nickel dopant in aqueous colloidal ZnS nanocrystals for efficient solar-driven CO_2 reduction. Appl Catal B: Environ 244:1013–1020. https://doi.org/10.1016/j.apcatb.2018.12.010
60. Liao L, Zhang Q, Su Z, Zhao Z, Wang Y, Li Y, Lu X, Wei D, Feng G, Yu Q, Cai X, Zhao J, Ren Z, Fang H, Robles-Hernandez F, Baldelli S, Bao J (2014) Efficient solar water-splitting using a nanocrystalline CoO photocatalyst. Nat Nanotechnol 9:69–73. https://doi.org/10.1038/nnano.2013.272
61. Liu Z, Ma C, Cai Q, Hong T, Guo K, Yan L (2017) Promising cobalt oxide and cobalt oxide/silver photocathodes for photoelectrochemical water splitting. Sol Energy Mater Sol Cells 161:46–51. https://doi.org/10.1016/j.solmat.2016.11.026
62. Liu G, Wang T, Zhang H, Meng X, Hao D, Chang K, Li P, Kako T, Ye J (2015) Nature-inspired environmental "Phosphorylation" boosts photocatalytic H_2 production over carbon nitride nanosheets under visible-light irradiation. Angew Chem Int Ed 54(46):13561–13565. https://doi.org/10.1002/anie.201505802

63. Liu G, Zhao G, Zhou W, Liu Y, Pang H, Zhang H, Hao D, Meng X, Li P, Kako T, Ye J (2016) In Situ bond modulation of graphitic carbon nitride to construct p–n homojunctions for enhanced photocatalytic hydrogen production. Adv Funct Mater 26(37):6822–6829. https://doi.org/10.1002/adfm.201602779
64. Liu W, Cao L, Cheng W, Cao Y, Liu X, Zhang W, Mou X, Jin L, Zheng X, Che W, Liu Q, Yao T, Wei S (2017) Single-site active cobalt-based photocatalyst with a long carrier lifetime for spontaneous overall water splitting. Angew Chem Int Ed 56(32):9312–9317. https://doi.org/10.1002/anie.201704358
65. Liu J, Liu Y, Liu N, Han Y, Zhang X, Huang H, Lifshitz Y, Lee S-T, Zhong J, Kang Z (2015) Metal-free efficient photocatalyst for stable visible water splitting via a two-electron pathway. Science 347(6225):970–974. https://doi.org/10.1126/science.aaa3145
66. Xu G, Zhang H, Wei J, Zhang H-X, Wu X, Li Y, Li C, Zhang J, Ye J (2018) Integrating the g-C_3N_4 nanosheet with B-H bonding decorated metal-organic framework for CO_2 activation and photoreduction. ACS Nano 12(6):5333–5340. https://doi.org/10.1021/acsnano.8b00110
67. Fang Y, Wang X (2018) Photocatalytic CO_2 conversion by polymeric carbon nitrides. Chem Commun 54(45):5674–5687. https://doi.org/10.1039/C8CC02046A
68. Ohno T, Murakami N, Koyanagi T, Yang Y (2014) Photocatalytic reduction of CO_2 over a hybrid photocatalyst composed of WO_3 and graphitic carbon nitride (g-C_3N_4) under visible light. J CO_2 Util 6:17–25. https://doi.org/10.1016/j.jcou.2014.02.002
69. Dong G, Ho W, Wang C (2015) Selective Photocatalytic N_2 fixation dependent on g-C_3N_4 Induced by nitrogen vacancies. J Mater Chem A 3(46):23435–23441. https://doi.org/10.1039/C5TA06540B
70. Zhu M, Kim S, Mao L, Fujitsuka M, Zhang J, Wang X, Majima T (2017) Metal-free photocatalyst for H_2 evolution in visible to near-infrared region: black phosphorus/graphitic carbon nitride. J Am Chem Soc 139(37):13234–13242. https://doi.org/10.1021/jacs.7b08416
71. Li H, Li J, Ai Z, Jia F, Zhang L (2018) Oxygen vacancy-mediated photocatalysis of BiOCl: reactivity, selectivity, and perspectives. Angew Chem Int Ed 57(1):122–138. https://doi.org/10.1002/anie.201705628
72. Li H, Shang J, Shi J, Zhao K, Zhang L (2016) Facet-dependent solar ammonia synthesis of BiOCl nanosheets via a proton-assisted electron transfer pathway. Nanoscale 8(4):1986–1993. https://doi.org/10.1039/C5NR07380D
73. Li H, Shang J, Ai Z, Zhang L (2015) Efficient visible light nitrogen fixation with BiOBr nanosheets of oxygen vacancies on the exposed 001 facets. J Am Chem Soc 137(19):6393–6399. https://doi.org/10.1021/jacs.5b03105
74. Wang S, Hai X, Ding X, Chang K, Xiang Y, Meng X, Yang Z, Chen H, Ye J (2017) Light-switchable oxygen vacancies in ultrafine Bi_5O_7Br nanotubes for boosting solar-driven nitrogen fixation in pure water. Adv Mater 29(31):1701774. https://doi.org/10.1002/adma.201701774
75. Kudo A, Miseki Y (2009) Heterogeneous photocatalyst materials for water splitting. Chem Soc Rev 38(1):253–278. https://doi.org/10.1039/B800489G
76. Takanabe K (2017) Photocatalytic water splitting: quantitative approaches toward photocatalyst by design. ACS Catal 7(11):8006–8022. https://doi.org/10.1021/acscatal.7b02662
77. Zhang L, Jaroniec M (2018) Toward designing semiconductor-semiconductor heterojunctions for photocatalytic applications. Appl Surf Sci 430:2–17. https://doi.org/10.1016/j.apsusc.2017.07.192
78. Yang J, Wang D, Han H, Li C (2013) Roles of cocatalysts in photocatalysis and photoelectrocatalysis. Acc Chem Res 46(8):1900–1909. https://doi.org/10.1021/ar300227e
79. Indrakanti VP, Kubicki JD, Schobert HH (2009) Photoinduced activation of CO_2 on Ti-based heterogeneous catalysts: current state, chemical physics-based insights and outlook. Energy Environ Sci 2(7):745–758. https://doi.org/10.1039/B822176F

80. Liu L, Zhao C, Li Y (2012) Spontaneous dissociation of CO_2 to CO on defective surface of Cu(I)/TiO_{2-x} nanoparticles at room temperature. J Phys Chem C 116(14):7904–7912. https://doi.org/10.1021/jp300932b
81. Rossmeisl J, Bessler WG (2008) Trends in catalytic activity for SOFC anode materials. Solid State Ionics 178(31):1694–1700. https://doi.org/10.1016/j.ssi.2007.10.016
82. Laursen AB, Varela AS, Dionigi F, Fanchiu H, Miller C, Trinhammer OL, Rossmeisl J, Dahl S (2012) Electrochemical hydrogen evolution: Sabatier's principle and the volcano plot. J Chem Educ 89(12):1595–1599. https://doi.org/10.1021/ed200818t
83. Pang H, Masuda T, Ye J (2018) Semiconductor-based photoelectrochemical conversion of carbon dioxide: stepping towards artificial photosynthesis. Chem Asian J 13(2):127–142. https://doi.org/10.1002/asia.201701596
84. Medford AJ, Vojvodic A, Hummelshøj JS, Voss J, Abild-Pedersen F, Studt F, Bligaard T, Nilsson A, Nørskov JK (2015) From the Sabatier principle to a predictive theory of transition-metal heterogeneous catalysis. J Catal 328:36–42. https://doi.org/10.1016/j.jcat.2014.12.033
85. Wang S, Ichihara F, Pang H, Chen H, Ye J (2018) Nitrogen fixation reaction derived from nanostructured catalytic materials. Adv Funct Mater 28(50):1803309. https://doi.org/10.1002/adfm.201803309
86. Hai X, Chang K, Pang H, Li M, Li P, Liu H, Shi L, Ye J (2016) Engineering the edges of MoS_2 (WS_2) crystals for direct exfoliation into monolayers in polar micromolecular solvents. J Am Chem Soc 138(45):14962–14969. https://doi.org/10.1021/jacs.6b08096
87. Wang P, Zhan S, Wang H, Xia Y, Hou Q, Zhou Q, Li Y, Kumar RR (2018) Cobalt phosphide nanowires as efficient Co-catalyst for photocatalytic hydrogen evolution over $Zn_{0.5}Cd_{0.5}S$. Appl Catal B: Environ 230:210–219. https://doi.org/10.1016/j.apcatb.2018.02.043
88. Chang K, Hai X, Pang H, Zhang H, Shi L, Liu G, Liu H, Zhao G, Li M, Ye J (2016) Targeted synthesis of 2H- and 1T-phase MoS_2 monolayers for catalytic hydrogen evolution. Adv Mater 28(45):10033–10041. https://doi.org/10.1002/adma.201603765
89. Fu J, Bie C, Cheng B, Jiang C, Yu J (2018) Hollow CoS_x polyhedrons act as high-efficiency cocatalyst for enhancing the photocatalytic hydrogen generation of g-C_3N_4. ACS Sustainable Chem Eng 6(2):2767–2779. https://doi.org/10.1021/acssuschemeng.7b04461
90. Attia Y, Samer M (2017) Metal clusters: new era of hydrogen production. Renew Sustain Energy Rev 79:878–892. https://doi.org/10.1016/j.rser.2017.05.113
91. Zhen W, Gao H, Tian B, Ma J, Lu G (2016) Fabrication of low adsorption energy Ni–Mo cluster cocatalyst in metal-organic frameworks for visible photocatalytic hydrogen evolution. ACS Appl Mater Interfaces 8(17):10808–10819. https://doi.org/10.1021/acsami.5b12524
92. Yamamoto M, Yoshida T, Yamamoto N, Nomoto T, Yamamoto Y, Yagi S, Yoshida H (2015) Photocatalytic reduction of CO_2 with water promoted By Ag clusters in Ag/Ga_2O_3 photocatalysts. J Mater Chem A 3(32):16810–16816. https://doi.org/10.1039/C5TA04815J
93. Cao Y, Chen S, Luo Q, Yan H, Lin Y, Liu W, Cao L, Lu J, Yang J, Yao T, Wei S (2017) Atomic-level insight into optimizing the hydrogen evolution pathway over a Co_1-N_4 single-site photocatalyst. Angew Chem Int Ed 56(40):12191–12196. https://doi.org/10.1002/anie.201706467
94. Zhao G, Liu H, Ye J (2018) Constructing and controlling of highly dispersed metallic sites for catalysis. Nano Today 19:108–125. https://doi.org/10.1016/j.nantod.2018.02.013
95. Zhang H, Wei J, Dong J, Liu G, Shi L, An P, Zhao G, Kong J, Wang X, Meng X, Zhang J, Ye J (2016) Efficient visible-light-driven carbon dioxide reduction by a single-atom implanted metal-organic framework. Angew Chem Int Ed 55(46):14310–14314. https://doi.org/10.1002/anie.201608597
96. Pinaud BA, Benck JD, Seitz LC, Forman AJ, Chen Z, Deutsch TG, James BD, Baum KN, Baum GN, Ardo S, Wang H, Miller E, Jaramillo TF (2013) Technical and economic feasibility of centralized facilities for solar hydrogen production via photocatalysis and photoelectrochemistry. Energy Environ Sci 6(7):1983–2002. https://doi.org/10.1039/C3EE40831K

97. Ryu A (2011) Development of a new system for photocatalytic water splitting into H_2 and O_2 under visible light irradiation. Bull Chem Soc Jpn 84(10):1000–1030. https://doi.org/10.1246/bcsj.20110132
98. Yoshida M, Takanabe K, Maeda K, Ishikawa A, Kubota J, Sakata Y, Ikezawa Y, Domen K (2009) Role and function of noble-metal/Cr-layer core/shell structure cocatalysts for photocatalytic overall water splitting studied by model electrodes. J Phys Chem C 113(23):10151–10157. https://doi.org/10.1021/jp901418u
99. Maeda K, Teramura K, Lu D, Saito N, Inoue Y, Domen K (2007) Roles of Rh/Cr_2O_3 (Core/Shell) nanoparticles photodeposited on visible-light-responsive $(Ga_{1-x}Zn_x)(N_{1-x}O_x)$ solid solutions in photocatalytic overall water splitting. J Phys Chem C 111(20):7554–7560. https://doi.org/10.1021/jp071056j
100. Maeda K, Domen K (2010) Photocatalytic water splitting: recent progress and future challenges. J Phys Chem Lett 1(18):2655–2661. https://doi.org/10.1021/jz1007966
101. Kato H, Kudo A (2003) Photocatalytic water splitting into H_2 and O_2 over various tantalate photocatalysts. Catal Today 78(1):561–569. https://doi.org/10.1016/S0920-5861(02)00355-3
102. Pan C, Takata T, Domen K (2016) Overall water splitting on the transition-metal oxynitride photocatalyst $LaMg_{1/3}Ta_{2/3}O_2N$ over a large portion of the visible-light spectrum. Chem Eur J 22(5):1854–1862. https://doi.org/10.1002/chem.201504376
103. Kobayashi R, Takashima T, Tanigawa S, Takeuchi S, Ohtani B, Irie H (2016) A heterojunction photocatalyst composed of zinc rhodium oxide, single crystal-derived bismuth vanadium oxide, and silver for overall pure-water splitting under visible light up to 740 nm. PCCP 18(40):27754–27760. https://doi.org/10.1039/C6CP02903E
104. Wang Q, Hisatomi T, Ma SSK, Li Y, Domen K (2014) Core/shell structured La- and Rh-codoped $SrTiO_3$ as a hydrogen evolution photocatalyst in Z-scheme overall water splitting under visible light irradiation. Chem Mater 26(14):4144–4150. https://doi.org/10.1021/cm5011983
105. Iwase A, Ng YH, Ishiguro Y, Kudo A, Amal R (2011) Reduced graphene oxide as a solid-state electron mediator in Z-scheme photocatalytic water splitting under visible light. J Am Chem Soc 133(29):11054–11057. https://doi.org/10.1021/ja203296z
106. Chen S, Qi Y, Hisatomi T, Ding Q, Asai T, Li Z, Ma SSK, Zhang F, Domen K, Li C (2015) Efficient visible-light-driven Z-scheme overall water splitting using a $MgTa_2O_{6-x}N_y$/TaON heterostructure photocatalyst for H_2 evolution. Angew Chem Int Ed 54(29):8498–8501. https://doi.org/10.1002/anie.201502686
107. Zong X, Wu G, Yan H, Ma G, Shi J, Wen F, Wang L, Li C (2010) Photocatalytic H_2 evolution on MoS_2/CdS catalysts under visible light irradiation. J Phys Chem C 114(4):1963–1968. https://doi.org/10.1021/jp904350e
108. Mikkelsen M, Jørgensen M, Krebs FC (2010) The teraton challenge. A review of fixation and transformation of carbon dioxide. Energy Environ Sci 3(1):43–81. https://doi.org/10.1039/B912904A
109. Ran J, Jaroniec M, Qiao S-Z (2018) Cocatalysts in semiconductor-based photocatalytic CO_2 reduction: achievements, challenges, and opportunities. Adv Mater 30(7):1704649. https://doi.org/10.1002/adma.201704649
110. Álvarez A, Borges M, Corral-Pérez JJ, Olcina JG, Hu L, Cornu D, Huang R, Stoian D, Urakawa A (2017) CO_2 activation over catalytic surfaces. ChemPhysChem 18(22):3135–3141. https://doi.org/10.1002/cphc.201700782
111. Olah GA, Prakash GKS, Goeppert A (2011) Anthropogenic chemical carbon cycle for a sustainable future. J Am Chem Soc 133(33):12881–12898. https://doi.org/10.1021/ja202642y
112. Chang X, Wang T, Gong J (2016) CO_2 photo-reduction: insights into CO_2 activation and reaction on surfaces of photocatalysts. Energy Environ Sci 9(7):2177–2196. https://doi.org/10.1039/C6EE00383D

113. Guo L-J, Wang Y-J, He T (2016) Photocatalytic reduction of CO_2 over heterostructure semiconductors into value-added chemicals. Chem Rec 16(4):1918–1933. https://doi.org/10.1002/tcr.201600008
114. Habisreutinger SN, Schmidt-Mende L, Stolarczyk JK (2013) Photocatalytic reduction of CO_2 on TiO_2 and other semiconductors. Angew Chem Int Ed 52(29):7372–7408. https://doi.org/10.1002/anie.201207199
115. Jia J, Qian C, Dong Y, Li YF, Wang H, Ghoussoub M, Butler KT, Walsh A, Ozin GA (2017) Heterogeneous catalytic hydrogenation of CO_2 by metal oxides: defect engineering—perfecting imperfection. Chem Soc Rev 46(15):4631–4644. https://doi.org/10.1039/C7CS00026J
116. Michalkiewicz B, Majewska J, Kądziołka G, Bubacz K, Mozia S, Morawski AW (2014) Reduction of CO_2 by adsorption and reaction on surface of TiO_2-nitrogen modified photocatalyst. J CO_2 Util 5:47–52. https://doi.org/10.1016/j.jcou.2013.12.004
117. Mao J, Peng T, Zhang X, Li K, Ye L, Zan L (2013) Effect of graphitic carbon nitride microstructures on the activity and selectivity of photocatalytic CO_2 reduction under visible light. Catal Sci Technol 3(5):1253–1260. https://doi.org/10.1039/C3CY20822B
118. Liu Q, Wu D, Zhou Y, Su H, Wang R, Zhang C, Yan S, Xiao M, Zou Z (2014) Single-crystalline, Ultrathin $ZnGa_2O_4$ nanosheet scaffolds to promote photocatalytic activity in CO_2 reduction into methane. ACS Appl Mater Interfaces 6(4):2356–2361. https://doi.org/10.1021/am404572g
119. Wang C, Xie Z, deKrafft KE, Lin W (2011) Doping metal-organic frameworks for water oxidation, carbon dioxide reduction, and organic photocatalysis. J Am Chem Soc 133(34):13445–13454. https://doi.org/10.1021/ja203564w
120. Liao Y, Cao S-W, Yuan Y, Gu Q, Zhang Z, Xue C (2014) Efficient CO_2 capture and photoreduction by amine-functionalized TiO_2. Chem Eur J 20(33):10220–10222. https://doi.org/10.1002/chem.201403321
121. Meng X, Ouyang S, Kako T, Li P, Yu Q, Wang T, Ye J (2014) Photocatalytic CO_2 conversion over alkali modified TiO_2 without loading noble metal cocatalyst. Chem Commun 50(78):11517–11519. https://doi.org/10.1039/C4CC04848B
122. Xie S, Wang Y, Zhang Q, Deng W, Wang Y (2014) MgO- and Pt-promoted TiO_2 as an efficient photocatalyst for the preferential reduction of carbon dioxide in the presence of water. ACS Catal 4(10):3644–3653. https://doi.org/10.1021/cs500648p
123. Liu H, Meng X, Dao TD, Zhang H, Li P, Chang K, Wang T, Li M, Nagao T, Ye J (2015) Conversion of carbon dioxide by methane reforming under visible-light irradiation: surface-plasmon-mediated nonpolar molecule activation. Angew Chem Int Ed 54(39):11545–11549. https://doi.org/10.1002/anie.201504933
124. Liu H, Li M, Dao TD, Liu Y, Zhou W, Liu L, Meng X, Nagao T, Ye J (2016) Design of PdAu alloy plasmonic nanoparticles for improved catalytic performance in CO_2 reduction with visible light irradiation. Nano Energy 26:398–404. https://doi.org/10.1016/j.nanoen.2016.05.045
125. Yu S, Wilson AJ, Heo J, Jain PK (2018) Plasmonic control of multi-electron transfer and C-C coupling in visible-light-driven CO_2 reduction on Au nanoparticles. Nano Lett 18(4):2189–2194. https://doi.org/10.1021/acs.nanolett.7b05410
126. Collado L, Reynal A, Coronado JM, Serrano DP, Durrant JR, de la Peña O'Shea VA (2015) Effect of Au surface plasmon nanoparticles on the selective CO_2 photoreduction to CH_4. Appl Catal B: Environ 178:177–185. https://doi.org/10.1016/j.apcatb.2014.09.032
127. Song H, Meng X, Dao TD, Zhou W, Liu H, Shi L, Zhang H, Nagao T, Kako T, Ye J (2018) Light-enhanced carbon dioxide activation and conversion by effective plasmonic coupling effect of Pt and Au nanoparticles. ACS Appl Mater Interfaces 10(1):408–416. https://doi.org/10.1021/acsami.7b13043
128. Linic S, Christopher P, Ingram DB (2011) Plasmonic-metal nanostructures for efficient conversion of solar to chemical energy. Nat Mater 10:911–921. https://doi.org/10.1038/nmat3151

129. Meng X, Liu L, Ouyang S, Xu H, Wang D, Zhao N, Ye J (2016) Nanometals for solar-to-chemical energy conversion: from semiconductor-based photocatalysis to plasmon-mediated photocatalysis and photo-thermocatalysis. Adv Mater 28(32):6781–6803. https://doi.org/10.1002/adma.201600305
130. Liu G, Meng X, Zhang H, Zhao G, Pang H, Wang T, Li P, Kako T, Ye J (2017) Elemental boron for efficient carbon dioxide reduction under light irradiation. Angew Chem Int Ed 56(20):5570–5574. https://doi.org/10.1002/anie.201701370
131. Lais A, Gondal MA, Dastageer MA, Al-Adel FF (2018) Experimental parameters affecting the photocatalytic reduction performance of CO_2 to methanol: a review. Int J Energy Res 42(6):2031–2049. https://doi.org/10.1002/er.3965
132. White JL, Baruch MF, Pander JE, Hu Y, Fortmeyer IC, Park JE, Zhang T, Liao K, Gu J, Yan Y, Shaw TW, Abelev E, Bocarsly AB (2015) Light-driven heterogeneous reduction of carbon dioxide: photocatalysts and photoelectrodes. Chem Rev 115(23):12888–12935. https://doi.org/10.1021/acs.chemrev.5b00370
133. Medford AJ, Hatzell MC (2017) Photon-driven nitrogen fixation: current progress, thermodynamic considerations, and future outlook. ACS Catal 7(4):2624–2643. https://doi.org/10.1021/acscatal.7b00439
134. Jia H-P, Quadrelli EA (2014) Mechanistic aspects of dinitrogen cleavage and hydrogenation to produce ammonia in catalysis and organometallic chemistry: relevance of metal hydride bonds and dihydrogen. Chem Soc Rev 43(2):547–564. https://doi.org/10.1039/C3CS60206K
135. Légaré M-A, Bélanger-Chabot G, Dewhurst RD, Welz E, Krummenacher I, Engels B, Braunschweig H (2018) Nitrogen fixation and reduction at boron. Science 359(6378):896–900. https://doi.org/10.1126/science.aaq1684
136. Chen X, Li N, Kong Z, Ong W-J, Zhao X (2018) Photocatalytic fixation of nitrogen to ammonia: state-of-the-art advancements and future prospects. Mater Horizons 5(1):9–27. https://doi.org/10.1039/C7MH00557A
137. Li J, Li H, Zhan G, Zhang L (2017) Solar water splitting and nitrogen fixation with layered bismuth oxyhalides. Acc Chem Res 50(1):112–121. https://doi.org/10.1021/acs.accounts.6b00523
138. Dhar NR, Pant NN (1944) Nitrogen loss from soils and oxide surfaces. Nature 153:115–116. https://doi.org/10.1038/153115a0
139. Schrauzer GN, Strampach N, Hui LN, Palmer MR, Salehi J (1983) Nitrogen photoreduction on desert sands under sterile conditions. Proc Natl Acad Sci U.S.A. 80(12):3873–3876. https://doi.org/10.1073/pnas.80.12.3873
140. Lindley BM, Appel AM, Krogh-Jespersen K, Mayer JM, Miller AJM (2016) Evaluating the thermodynamics of electrocatalytic N_2 reduction in acetonitrile. ACS Energy Lett 1(4):698–704. https://doi.org/10.1021/acsenergylett.6b00319
141. van der Ham CJM, Koper MTM, Hetterscheid DGH (2014) Challenges in reduction of dinitrogen by proton and electron transfer. Chem Soc Rev 43(15):5183–5191. https://doi.org/10.1039/C4CS00085D
142. Jacobsen CJH, Dahl S, Clausen BS, Bahn S, Logadottir A, Nørskov JK (2001) Catalyst design by interpolation in the periodic table: bimetallic ammonia synthesis catalysts. J Am Chem Soc 123(34):8404–8405. https://doi.org/10.1021/ja010963d
143. Zhu D, Zhang L, Ruther RE, Hamers RJ (2013) Photo-illuminated diamond as a solid-state source of solvated electrons in water for nitrogen reduction. Nat Mater 12:836–841. https://doi.org/10.1038/nmat3696
144. Bell AT (2003) The impact of nanoscience on heterogeneous catalysis. Science 299(5613):1688–1691. https://doi.org/10.1126/science.1083671
145. Matanović I, Garzon FH, Henson NJ (2014) Electro-reduction of nitrogen on molybdenum nitride: structure, energetics, and vibrational spectra from DFT. PCCP 16(7):3014–3026. https://doi.org/10.1039/C3CP54559H

146. Zhao Y, Zhao Y, Waterhouse GIN, Zheng L, Cao X, Teng F, Wu L-Z, Tung C-H, O'Hare D, Zhang T (2017) Layered-double-hydroxide nanosheets as efficient visible-light-driven photocatalysts for dinitrogen fixation. Adv Mater 29(42):1703828. https://doi.org/10.1002/adma.201703828
147. Skúlason E, Bligaard T, Gudmundsdóttir S, Studt F, Rossmeisl J, Abild-Pedersen F, Vegge T, Jónsson H, Nørskov JK (2012) A theoretical evaluation of possible transition metal electrocatalysts for N_2 reduction. PCCP 14(3):1235–1245. https://doi.org/10.1039/C1CP22271F
148. Abghoui Y, Garden AL, Hlynsson VF, Björgvinsdóttir S, Ólafsdóttir H, Skúlason E (2015) Enabling electrochemical reduction of nitrogen to ammonia at ambient conditions through rational catalyst design. PCCP 17(7):4909–4918. https://doi.org/10.1039/C4CP04838E
149. Li H, Shi J, Zhao K, Zhang L (2014) Sustainable molecular oxygen activation with oxygen vacancies on the 001 facets of BiOCl nanosheets under solar light. Nanoscale 6(23):14168–14173. https://doi.org/10.1039/C4NR04810E
150. Ali M, Zhou F, Chen K, Kotzur C, Xiao C, Bourgeois L, Zhang X, MacFarlane DR (2016) Nanostructured photoelectrochemical solar cell for nitrogen reduction using plasmon-enhanced black silicon. Nat Commun 7:11335. https://doi.org/10.1038/ncomms11335